HIGH PERFORMANCE RESISTOJET THRUSTER: STAR STATUS UPDATE

BARCELO RENACIMIENTO HOTEL, SEVILLE, SPAIN / 14 – 18 MAY 2018

Federico Romei [(1)], Angelo Grubišić [(2)], Matt Robinson [(3)], Dave Gibbon [(4)] Paul Aimone [(5)] and Francois Dary [(6)]

[(1,2,3)] University of Southampton, University Road, Southampton, SO171BJ, UK, f.romei@soton.ac.uk; a.grubisic@soton.ac.uk; m.d.robinson@soton.ac.uk;

[(3)] Surrey Satellite Technology Ltd., Tycho House, 20 Stephenson Road, Surrey Research Park, Guildford, Surrey GU2 7YE, UK, d.gibbon@sstl.co.uk

[(4,5)] H.C. Starck Inc., 45 Industrial Place, Newton, MA, 02461, USA paul.aimone@hcstarck.com; francois.dary@hcstarck.com

KEYWORDS: resistojet, prototype, spacecraft, propulsion, metal additive manufacturing, stainless steel, performance, tantalum.

ABSTRACT:

This paper presents the performance testing of the Super-high Temperature Additive Resistojet (STAR) prototype, the first additively manufactured resistojet thruster with a novel monolithic design of heat exchanger. In this paper, operation of the concept was demonstrated at the operational temperature limits of the prototype material. In hot gas mode, the prototype developed 80s specific impulse with argon gas, with a calculated stagnation temperature between 380°C and 500°C at the inlet of the nozzle. The paper proves the feasibility of operation of a concentric thin walled monolithic recirculating resistojet manufactured via selective laser melting.

1. INTRODUCTION

The primary driver of resistojet technology is a requirement for the all-electric propulsion spacecraft bus with common xenon propellant [1,2]. Geostationary telecommunication satellites typically use chemical propulsion for attitude control as well as orbit-raising and station-keeping. The benefit of using a high temperature resistojet is to optimise propellant mass fractions giving fuel load reduction, cost savings in launch vehicle option for lighter spacecraft and further reduction of integration and testing costs by eliminating the use of hazardous propellants. A second driver of the resistojet technology is the small Low Earth Orbit (LEO) platform. These satellites have limited resources, such as low volume and power budgets, therefore, they depend upon high propellant storage density – ISP product, and rely on inert propellants to lower assembly integration and testing (AIT) costs. The resulting propulsion system has low ISP, low total impulse and therefore limited onorbit/deorbit capability [3].

The STAR (Super-high Temperature Additive-manufactured Resistojet) thruster meets both of the applications described above. This paper presents the performance test on a prototype model, which has comparable performance to the xenon resistojet of SSTL [4]. The initial tests on the STAR prototype were influenced by a seal failure [5]. This paper presents a similar performance test but with the following improvement: the prototype assembly is hermetically sealed; thermal drift on the thrust measurements has been eliminated by using novel liquid-metal electrical terminal for power transfer to the thruster, as discussed in section 3.3.

1.1. Status of the project

Figure 1 shows a flowchart of the STAR development strategy at the University of Southampton. Currently this technology is at TRL of 3. In this paper, a development model thruster manufactured in 316L stainless steel has successfully been tested in laboratory environment. With this test campaign the novel concept of monolithic concentric tubular heat exchanger with integrated nozzle has been finally proven to work as expected. The next phase of the project consists of implementing different materials suitable for the high-temperature application. In particular, an engineering model made in tantalum is currently under production, while tantalum/tungsten alloys will be also investigated. In addition, Inconel alloys

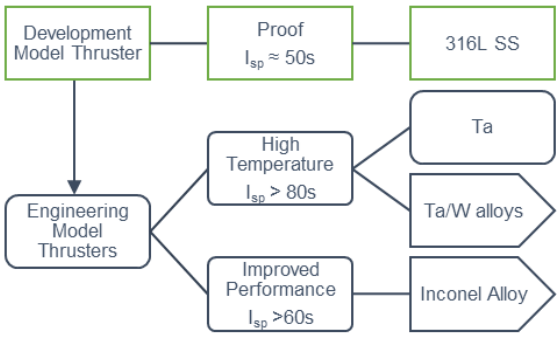

Figure 1. Technology roadmap of the STAR thruster with expected performance in terms of specific impulse using xenon propellant.

are considered for the production of an improved performance thruster with respect to the SSTL resistojet, which provides 48s of specific impulse. The latter offers better electrical compatibility with the spacecraft bus and is also compatible with iodine, suggesting a possible future application of the STAR thruster with the first candidate among the alternative propellants for electric propulsion [6,7].

Robinson [8] presents a thermal cycling test at high current (25 A), performed on a second identical prototype STAR thruster. This investigation shows a failure mode of the heat exchanger, which is described with the aid of X-ray Computed Tomography.

A tantalum heat exchanger, with identical geometry of the current prototype, has been successfully manufactured. Ogunlesi [9] presents the inspection of this component using both optical profilometry and CT scanning and put the tantalum and the stainless steel prototypes in comparison. This analysis demonstrates there are not apparent shortcoming in producing a STAR engineering model using tantalum.

2. PROTOTYPE MANUFACTURING

Figure 2 shows a CAD exploded view of the STAR thruster, with the main components identified. Table 1 reports the material and manufacturing process for the main parts. The Heat Exchanger and Thruster Inflow are manufactured via Selective Laser Melting using a Concept Laser M2 Cusing printer, while the remaining components are manufacture conventionally. All metallic components have been produced at the Faculty of engineering and the Environment Engineering Design and Manufacturing Centre at the University of Southampton. The assembly also include two Electron Beam welds to electrically couple the Heat Exchanger with the Thruster Inflow, at the height of the Collar, and the Heat Exchanger with the Casing, at the top surface of the thruster.

Figure 3 shows a radiograph inspection of the thruster assembly prior testing. The heat exchanger

Table 1. List of the main components of the STAR thruster with materials and manufacturing process specified.

Component	Material	Manufacturing process
Heat Exchanger	316L SS	Selective Laser Melting
Thruster Inflow	316L SS	Selective Laser Melting
Casing	316L SS	Machined
Support	316L SS	Machined
Collar	Macor	Machined
Nozzle Spacer	Shapal	Machined
Ceramic thermal spacers	Macor	Machined

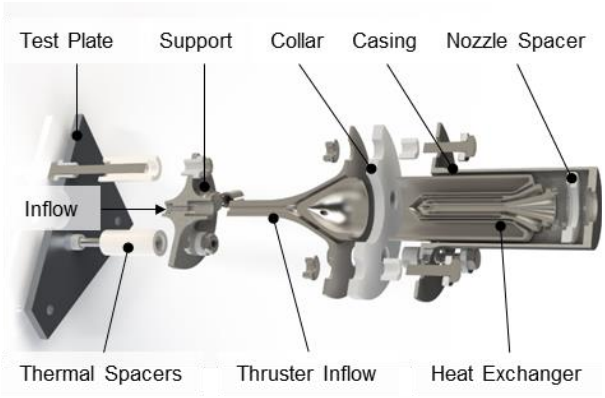

Figure 2. Exploded view of the STAR thruster assembly.

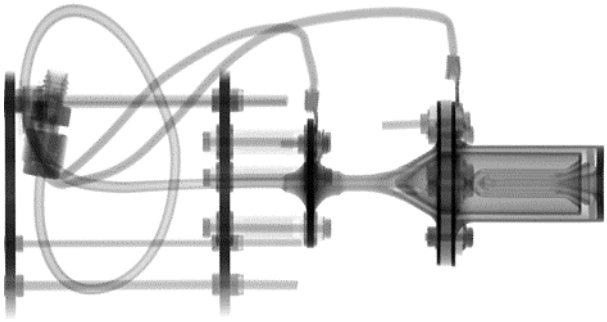

Figure 3. Radiograph of the STAR assembly showing the recirculating flow path reaching the nozzle.

appears as expected. The propellant enters through a 1/8'' stainless steel pipe, which is silver brazed onto the thruster inflow. The flow is then directed into an initial annular section obtained by the heat exchanger external wall and the thruster casing internal wall. After three more annular passages, the propellant enters an inner pipe element and it is finally expanded through the integrated converging-diverging nozzle. Electrical current is applied using ring terminals at the Casing and at the Support. The resulting dissipative heating, primarily in the inner four cylinders of the heat exchanger, heats the propellant progressively through the recirculating flow path.

3. PERFORMANCE TESTING METHODOLOGY

The thruster is characterized at a constant flow rate of argon propellant, in both cold gas mode and at a range of electrical current levels in current controlled mode. The stagnation temperature reached in the experiment is inferred from the experimental data.

3.1. Definition of Parameters

Eq.1 shows the expression of the electrical resistance, R, as function of the material resistivity, ρ, the conductor length, l, and the cross-section area. The STAR heat exchanger is designed to exert the most of the Joule heating in the inner four cylinders. From the innermost to outermost cylinder, the proportion of electrical resistance is

approximately 35%, 28%, 19% and 9% when cold, where the casing and the outer heat exchanger wall constitute most of the remaining resistance (< 9%).

$$R = \rho \frac{l}{A} \qquad \text{Eq.1}$$

The quantities directly measured in the experiment are: mass flow rate, $\dot{m}$, pressure measure at the pressure controller, p_{PC}, thrust, F, voltage and current, V and I respectively. The remaining quantities are derived analytically. The specific impulse is derived using Eq.2 from thrust, mass flow rate and acceleration due to gravity, g_0.

$$I_{sp} = \frac{F}{\dot{m} g_0} \qquad \text{Eq.2}$$

Eq.3 is used instead to infer the stagnation temperature of the gas at the inlet of the converging-diverging nozzle, where the specific heat of argon is c_p = 520 Jkg^{-1}K^{-1}, η_n is the nozzle efficiency and I_{sp}^* is the ideal specific impulse of a 1-D adiabatic nozzle.

$$I_{sp} \approx \frac{\eta_n}{g_0}\sqrt{2 c_p T_t} = \eta_n I_{sp}^* \qquad \text{Eq.3}$$

Finally, Eq.4 is used to calculate the thruster efficiency, η_{ts}, expressed as the product of the heat exchanger efficiency, η_h, and the nozzle efficiency. P_t is the stagnation power associated with the gas at the inlet of the nozzle, P_j is the kinetic power at the exit of the nozzle, P_0 is the power associated to the inlet cold gas, P_e is the electrical power and V_j is the exhaust velocity.

$$\eta_{ts} = \eta_h \eta_n = \frac{P_t}{P_{ts}}\frac{P_j}{P_t} = \frac{P_j}{P_{ts}} = \frac{\frac{1}{2}\dot{m} V_j^2}{P_0 + P_e} \qquad \text{Eq.4}$$

The total gas power, P_{ts}, is the sum of the electrical power and the cold gas power, , where T_0 is the cold gas power at inlet of the thruster.

$$P_0 = \dot{m} c_p T_0 \qquad \text{Eq.5}$$

3.2. Test Setup

The STAR breadboard model was tested in the David Fearn Electric Propulsion Laboratory at the University of Southampton, Figure 4. This facility has a main test chamber 4m long by 2m diameter, pumped by two cryopumps, 3 turbomolecular pumps and 2 backing pumps, maintaining less than 5.5 x 10^{-5} mbar up to 30 sccm xenon and with a base pressure of < 9 x 10^{-8} mbar. The test item is placed in the small hatch of the chamber, which can be isolated from the test chamber via a gate valve. This allows rapid test set up and preparation followed by

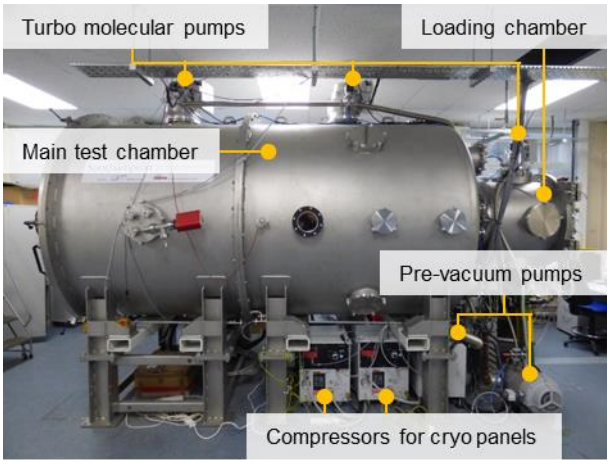

Figure 4. Overview of the David Fearn Electric Propulsion Laboratory at the University of Southampton with main components labelled.

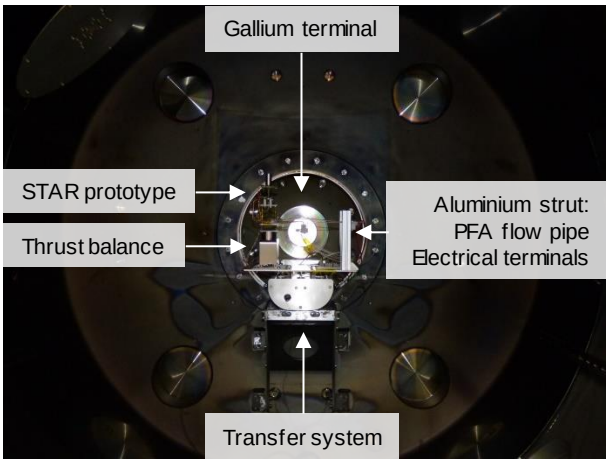

Figure 5. Test rig with thruster located vertically in the main test chamber.

retest. The test results presented in this paper are performed with the gate valve opened and the thruster positioned into the main test chamber through a transfer trolley from the hatch (Figure 5).

Thrust is directly measured with a Mettler Toledo weighing module, with the resistojet mounted vertically. The 1/8'' stainless steel inflow pipe and the electrical terminal are fixed on a second aluminium configuration plate, to avoid their thermal effects on the thrust measurement. Argon is supplied to the thruster via a 1/8'' PFA flexible pipe, which is fixed on a levelled aluminium strut on the opposite end of the thruster. Likewise, the high-current cables are fixed on an aluminium strut. In this way, any flexural force on the balance of the PFA pipe or of the terminal cables is kept to a minimum. In addition, a liquid-metal electrical terminal is used to avoid the thermal drift observed in the thrust measurements of the previous test campaign [5].
A Bronkhorst based flow system provides mass flow controlled inflow to the thruster. The flow system is connected to both the Ar cylinder and to the chamber feedthrough with 1/4'' stainless steel hoses. A high-current DC power supply is used in

current controlled mode and thruster voltage is monitored through an oscilloscope. Thrust balance, flow system, power supply, gallium terminal heaters and thermocouples are connected to a workstation, via a DAQ system, and controlled using a LabVIEW interface.

3.3. Gallium Electrical Terminals

The Gallium electrical terminals were conceived to avoid any thermal drift on the thruster balance due to the expansion of the high-current cables, which is significant (shown in [5]). Gallium is a non-toxic metal, suitable for vacuum and with a low melting point of about 30°C. The electrical terminal consists of two stainless steel baths, each one with a 10W cartridge heater inserted in the body (Figure 6). Each bath contains about 8 grams of gallium, which is melted by heating the baths at 35°C with a hysteresis cycle of ± 0.5°C. Two 1/8'' copper rods are connected to the thruster positive and negative terminal and immersed in the liquid gallium. During operation, the rods are unconstrained under thermal expansion, thus not influencing the thrust measurement.

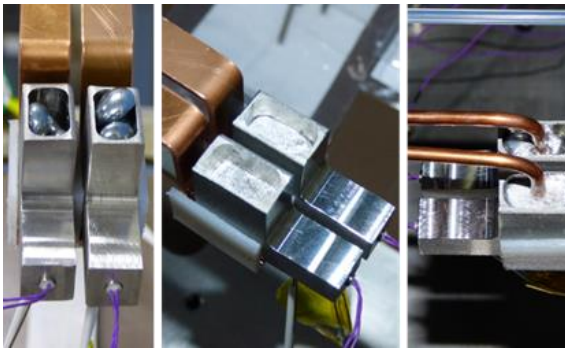

Figure 6. Gallium electrical terminal with: solid shots (left), melted metal (centre) and electrical terminals submerged in the liquid Gallium (right).

3.4. Test Method

The tests method of operation consisted of the following process steps to avoid over heating of the component:

1. The thruster is set in cold gas mode, with a heater current of 3A, which corresponds to a negligible power dissipation of 0.3W. In this way, the electrical resistance can be accurately measured in cold gas mode via voltage measurement at the thruster terminals.

Table 2. Performance data of the STAR prototype at two different mass flow rates of argon performed in vacuum at a base pressure of 8.5e-4 mbar.

Sym.	Unit	Ref.	Test number									
			1	2	3	4	5	6	7	8	9	10
$\dot{m}$	mg/s	-	18.84	18.84	18.84	18.84	18.84	38.44	38.44	38.44	38.44	38.44
F	mN	-	9.7	11.8	12.8	13.9	14.8	20.3	24.9	26.6	27.6	29.8
I_{sp}	s	Eq.2	53.62	63.88	69.34	75.25	79.58	54.11	66.37	70.90	73.56	79.42
P_e	W	$V \cdot I$	0.3	8.13	12.75	17.88	23.56	0.3	12.56	16.01	19.39	22.65
R	mΩ	$V \,/\, I$	33.3	36.5	38	40.1	42.3	33.3	35.6	37	38.9	40.6
V	V	-	0.1	0.546	0.696	0.847	0.998	0.1	0.532	0.678	0.821	0.959
I	A	-	3	14.9	18.3	21.1	23.6	3	14.9	18.3	21.1	23.6
P_{ts}	W	$P_0 + P_e$	3.2	15.75	19.33	22.89	26.45	3.2	18.49	21.92	25.29	28.55
η_{ts}	%	Eq.4	87.0	26.5	22.5	22.4	22.0	87.6	43.8	42.1	39.2	40.5
t_h	s	-	0	123.9	78.9	97.3	118.4	0	200	200	200	200
p_{PC}	bar	-	0.652	0.813	0.867	0.942	1.01	1.277	1.549	1.655	1.714	1.855
$T_{t,\min}$	°C	Eq.3, $\eta_n = 0.87$	20	142	215	302	379	20	170	233	272	362
$T_{t,\max}$	°C	Eq.3, $\eta_n = 0.95$	20	221	309	413	505	20	256	331	377	485

- Measured quantity.

Note: All values in this table are the maximum reached at each current level

2. The mass flow controller is set to the desired mass flow rate;
3. When the thrust reaches a steady value, the thruster is switched to hot gas mode, by increasing the electrical current to the prescribed level;
4. The current is decreased to the cold gas mode after the time of heating, t_h, elapsed;
5. The flow controller is closed.

4. RESULTS

The thrust measurement is obtained simply by converting the measured weight observed by the thrust balance. The error on the direct measurement was estimated from the manufacturer datasheet in the worst-case scenario, such as using the limit values rather than the typical values, and it is calculated as the sum of the following terms:

- 0.1 mg: repeatability (at nominal load);
- 0.4 mg: linearity deviation;
- 2 mg: sensitivity offset with a test load of 400g;
- 0.00015%/°C: sensitivity temperature drift;
- 0.00025%/a: sensitivity stability.

In this calculation, the sensitivity to temperature drift and stability are not taken into account. In addition, the readability is 0.1 mg ≈ 10 uN, therefore the balance reading in mN is in the form x.x mN. The resulting uncertainty is of ± 0.25 mN.

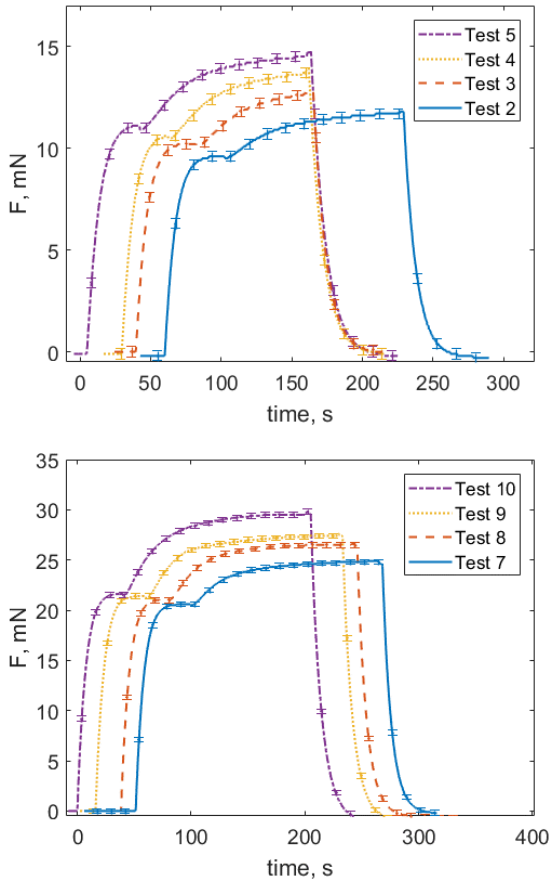

Figure 7. Thrust transient with 18.84 mg/s (top) and 38.44 mg/s (bottom) of argon for four electrical current levels. Error bar of the thrust measurement is shown.

Table *2* shows a summary of the performance data in terms of the maximum values reached at each test point. Tests 1 to 5 are performed at flow rate of 18.84 mgs^{-1}, while tests 6 to 10 are at 38.44 mgs^{-1}. The thruster has been tested with five increasing current levels at both flow rates. Test 1 and Test 6 correspond to the cold gas mode of the thruster, with 3 A of current and only 0.3W of electrical power. Direct measurements are indicated with a dash line, while a formula for the reaming quantities is shown in the reference column.

Figure 7 shows the thrust curve corresponding to each hot-gas test. For clarity, the curves are overlaid with a 20 seconds separation. The switch of electrical current to hot gas mode is clearly visible by the sharp increase of thrust in each test. The values reported in
Table *2* correspond to the last measurement taken at t_h, which also correspond to the maximum thrust.

5. DISCUSSION

The test method (section 3.4) consisted of reaching the cold gas steady-state thrust level before applying high current to avoid overheating. Tests 1 to 5 were performed in rapid sequence. Then, once the thruster had completely cooled, Tests 6 to 10 were also performed in rapid sequence. At both flow rates tests, from Test 2 to 5 and from Test 7 to 10 respectively, the thruster did not have time to cool to the initial ambient temperature. Therefore, the cold gas thrust increases at every subsequent current level (Figure 7). The time to reach the steady-state thrust for Test 1 is 31.98s, while for Test 6 it is 37.31s. However, this time is dependant on the response time of the flow system used, therefore should not be considered as a characteristic of the STAR thruster at this stage, until operated in a pressure controlled mode.

It can be noted that the thruster efficiency increases considerably at the highest flow rate (Test 6-10). This can be seen by considering Eq.4. Since the electrical power remains approximately unchanged between the two flow rates at the respective currents and the temperature distribution across the thruster must be also similar, therefore the losses in terms of radiation from the casing and conduction to the thruster stand are likely comparable. However, the useful kinetic power increases significantly due to of the higher flow rates, resulting in a higher thruster efficiency.

The thruster total efficiency, η_{ts} in the cold gas mode is 87% in Test 1, and of 87.6% in Test 6. In the assumption of a perfect heat exchanger, $\eta_h = 1$, the resulting nozzle efficiency is $\eta_n = \eta_{ts}$. In reality, the theoretical nozzle efficiency can be as high as 95%.

With the above two assumptions, the lower and upper bounds of the gas stagnation temperature at the nozzle inlet can be estimated using Eq.3.

The experiments were performed at constant current, which does not correspond to a constant power, since the thruster temperature increases in time and, consequently, the electrical resistance increases, and hence so does power. For this reason, the time to reach a steady hot mode thrust was higher with respect to a constant power mode. However, particularly for Tests 7-10, it can be observed that the thrust increases significantly at the instant of the electrical current application, then reaches a plateau. As an example, in test 10 the specific impulse is increased to the 90% of the final value, which corresponds to 75s specific impulse, in only 65 seconds. If the thruster is require to reach the desired thrust in less time, this can be achieved with a pre-heating operation.

In conclusion, the STAR prototype performed as expected and builds the basis for the next phases of the research project: to develop new thrusters using refractory metals and Inconel.

ACKOLEDGMENTS

Part of this research was funded by the Doctoral Training Partnership through the Engineering and Physical Sciences Research Council (EPSRC), grant no. EP/M50662X/1. This work was also supported by Innovate UK in the CEOI-ST National Space Technology Programme (NSTP-2), as part of the High Performance Xenon Resistojets project and in partnership with Surrey Satellite Technology Limited as an end-user of the technology. Additional funding was provided by the National Space Technology Programme (NSTP-3) from the UK Space Agency, as part of the RADICAL (Refractory Additive Layer Manufacturing for Commercial Space Applications) project.

The authors would also like to thank the beam scientists Dr. Sharif Ahmed and Dr. Kathryn Rankin of the μ-VIS X-Ray Imaging Centre for their technical support on the non-destructive inspection of the thruster assembly. Finally, the authors would like to thank Kevin Smith, the Faculty Production Facility Manager, and Richard Dooler, Additive Manufacturing Programmer, of the EDMC workshop of the University of Southampton for their technical contribution on the prototype production.

REFERENCES

1. Grubisic, A. N., & Gabriel, S. B. (2016). Assessment of the T5 and T6 Hollow Cathodes as Reaction Control Thrusters. *Journal of Propulsion and Power*(null), 1-11.
2. Coletti, M., Grubisic, A., Collingwood, C., & Gabriel, S. (2011). Electric propulsion subsystem architecture for an all-electric spacecraft. In *Advances in Spacecraft Technologies*: InTech.
3. Romei, F., Grubišić, A. N., & Gibbon, D. (2017). Manufacturing of a high-temperature resistojet heat exchanger by selective laser melting. *Acta Astronautica, 138*, 356-368. doi:https://doi.org/10.1016/j.actaastro.2017.05.020
4. Nicolini, D., Robertson, D., Chesta, E., Saccoccia, G., Gibbon, D., & Backer, A. (2003). *Xenon Resistojets as Secondary Propulsion on EP Spacecrafts and Performance Result of Resistojet Using Xenon*. Paper presented at the 28th International Electric Propulsion Conference, Toulouse, France.
5. Romei, F., Grubisic, A., & Gibbon, D. (2017). *Performance testing and evaluation of a high temperature xenon resistojet prototype manufactured by selective laser melting*. Paper presented at the International Electric Propulsion Conference, Atlanta.
6. Polzin, K. A., Seixal, J. F., Mauro, S. L., Burt, A. O., Martinez, A., & Martin, A. K. (2017). *The iodine Satellite (iSat) Propellant Feed System-Design and Development*. Paper presented at the International Electric Propulsion Conference, Atlanta.
7. Mazouffre, S. (2016). Electric propulsion for satellites and spacecraft: established technologies and novel approaches. *Plasma Sources Science and Technology, 25*(3), 033002.
8. Robinson, M., Ogunlesi, C., Grubisic, A., & Romei, F. (2018). Environmental and endurance testing of the STAR additively manufactured resistojet.
9. Ogunlesi, C., Robinson, M., Romei, F., & Grubisic, A. (2018). Novel non-destructive inspection of the STAR additively manufactured resistojet.